RSC Advances

RSC Advances

www.rsc.org/advances

ROYAL SOCIETY OF CHEMISTRY

www.rsc.org/advances

New understanding in the influence of melt structure and

β-nucleating agents on the polymorphic behavior of isotactic

polypropylene

Jian Kang[1], Gengsheng Weng[2], Zhengfang Chen[1], Jinyao Chen[1], Ya Cao[1], Feng Yang[1,*], Ming Xiang[1]

[1] State Key Laboratory of Polymer Materials Engineering, Polymer Research Institute of Sichuan University, Chengdu 610065, People's Republic of China

[2] Faculty of Materials and Chemical Engineering, Ningbo University, Ningbo 315211, People's Republic of China.

*Corresponding author's e-mail address: yangfengscu@126.com;

Abstract

The β-nucleation behavior of isotactic polypropylene (iPP) is a fascinating and important issue in polymer physics, however, neither enough phenomenon nor its physical nature has been clearly understood. In this study, by tuning the heating temperature (fusion temperature, T_f), the amount of ordered structures in iPP melt was controlled. In this way, the influence of five types of representative β-nucleating agent (β-NA) on the crystallization behavior of iPP with different melt structures (i.e. the amount of ordered structures) were comparatively studied by differential scanning calorimetry (DSC), polarized optical microscopy (PLOM), scanning electronic microscopy (SEM), wide-angle X-ray diffraction (WAXD) and rheological measurement. Surprising synergetic effect was observed between the β-NAs with α-/β-dual polymorphic selectivity (dual-selective β-NA) and the ordered structure of iPP, resulting in significant increase of the β-nucleation efficiency and the β-phase proportion of the sample. PLOM observation of the crystallization process confirmed that with the presence of ordered structures in iPP melt, mass of dark, small crystal embryos derived from self-nuclei uniformly distributed in the melt and exhibited β-nucleation efficiency. This work provided first evidence that for iPP nucleated with

1

dual-selective β-NA, the ordered structures play a determining role in the β-nucleation of iPP. Under the influence of the dual-selective β-NA, the ordered structures exhibited β-nucleation efficiency and therefore encouraged the β-nucleation. A possible mechanism was proposed.

Keywords: β-nucleated isotactic polypropylene; ordered structures; β-nucleation

1. Introduction

Polymer crystallization is a long-standing challenge in polymer physics attracting broad interests from scientific and industrial aspects owning to its great importance. During the last 60 years, great attention has been paid and many different theories or models have been developed [1, 2], however no full agreement was reached.

In the early stage of polymer crystallization, whether the ordered structure exists in the melt before the occurrence of the real crystallization or not is an important issue under debate [1-8]. A widely accepted viewpoint proposes that polymer chains in the melt are in a random coil state at high temperature, which will not form any ordered structures even at the level approaching the diameter of the chains. However, more and more experimental results indicate that some ordered structures may exist in supercooled polymer melt before the occurrence of real crystallization[9-14]. In induction period, a spinodal assisted crystallization mechanism has been proposed mainly based on the scattering and spectral results; at the growth front, Strobl G [1] proposed a multistage process model, where a transient mesomorphic layer is proposed at the growth front of crystal. Li LB [15, 16] studied the role of ordered structures in the growth front of isotactic polypropylene (iPP) and observed a growth front layer with ordered long helices outside the growth front of spherulite. The results showed the presence of preordering on the growth front of iPP spherulite.

It is reported that the locally ordered structures can also be created by other methods such as self-nucleation[17-21]. When the heating temperature (fusion temperature, T_f) is not high enough to make the polymer melt fully melting, an amount of ordered structures will survive within the melt. Therefore, the content of locally ordered structures can be tuned by controlling the T_f applied on the polymer.

Although the physical nature of the ordered structures is still under debate[22], it is commonly accepted that they can serve as self-nucleating agent during the crystallization process, enhance the nucleation density and crystallization rate [17, 22, 23].

As a typical semi-crystalline polymer and one of the most widely used commercial polymers, iPP exhibits pronounced polymorphisms and morphologies[24-29], which can crystallize into several crystal modifications known as monoclinic α-form[30], trigonal β-form[31-33] and orthorhombic γ-form[34]. The β-form is metastable crystalline phase and can be obtained only under several specific conditions such as shearing[35], using specific nucleating agents[36-44] and directional crystallization in thermal gradient[45]. Although the role of ordered structures in the α-phase crystallization of iPP has been well recognized, the relationship between the ordered structure and the β-crystallization has rarely been reported.

Recently, by introducing partially melting iPP fiber to homogeneous supercooled iPP melt, Yan SK et al.[46-50] systematically investigated the β-crystallization of iPP/iPP fiber single composite, and claimed that the partly melting of orientated fibers may provide the locally ordered structures within certain orientation window, which play very important role in the β-crystallization; Alfonso GC et al.[51-53] studied the formation and relaxation of shear-induced nucleation and found that shear flow and partially molten fiber have similar effect on the formation of β-phase; Shen CY et al.[54, 55] explored the combined effect of ordered structures and shear flow on polymorphic nature of β-cylindrites, and found that only in the presence of ordered structures can the iPP melt form β-cylindrites under the influence of shear flow, showing that the ordered structures under shearing is crucial to the β-crystallization of iPP. Although the crystallization conditions and components of the above works are quite different from each other, it should be emphasized that the two-stage characteristics of the β-nucleation in these studies are, to some extent, very similar: (i) at the early stage of crystallization, the row nucleated α-lamellae forms firstly along the shear stress / fiber direction. (ii) Then the β-nucleation takes places on the edge of the row nucleated α-lamellae, and a competitive growth of both α- and β-crystal occurs.

The above works make breakthroughs in relating the ordered structures to the

β-crystallization of iPP, and provide a possibility that by applying certain orientation status, these ordered structures might exhibit β-nucleation efficiency and therefore encourage the β-crystallization. However, to our best knowledge, it seems that in the quiescent iPP melt without shearing or orientated fibers, the role of the ordered structures in the β-nucleation of iPP is still not recognized; neither the phenomenon nor the general nature of the β-crystallization of iPP in different crystallization conditions (i.e., shearing, thermal gradient and β-nucleating agents) is clearly understood, which still needs further investigation.

The addition of β-nucleating agent (β-NA) is a commonly used method to enhance β-crystallization of iPP. Due to the limitation of the characterization techniques and the distinct characteristics of various β-NAs such as chemical constitution, polymorphic selectivity, β-nucleation efficiency and geometric shape [36, 38], the β-nucleation mechanism of the β-NAs is still not clear enough although some important theories such as the epitaxial crystallization mechanism had been proposed[56]. But on the other side, various NAs with distinct characteristics provide us an opportunity to tune their influence on the ordered structures of iPP, namely, a possibility to tune the β-nucleation efficiency of the ordered structures.

By investigating the β-crystallization behavior of the nucleated iPP with different melt structures (i.e. different contents of ordered structures), this study aims to explore the influence of various NAs on the ordered structures in iPP melt, so as to elucidate novel understanding in the role of ordered structures in β –nucleation of quiescent iPP melt, as well as the induction mechanism of β-NA in the β-crystallization of iPP.

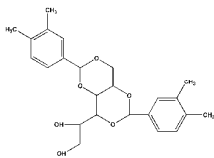## 2. Experimental Section

2.1 Materials
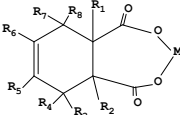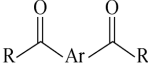
iPP, tradename T38F (Lanzhou OilChem Corp., China) with average isotacticity 97.6%, weight molecular weight 347200, polydispersity index=3.63, was used.

The five nucleating agents (NAs) used in this study are commercially available products, which are widely used and extensively studied in previous works. The detailed information of the NAs including tradename, manufacturer, chemical

composition, polymorphic selectivity were listed in Table 1. Moreover, their geometric shapes are observed by SEM as shown in Figure 1.

As can be seen from Figure 1 and Table I, the five NAs can be classified into different groups: According to the polymorphic selectivity, DMDBS is high efficient α-NA[39], meanwhile, Pa-Ca and NAB83 are β-NA with β-single polymorphic selectivity [44, 57], DCNDCA and WBG-II are β-NA with α-/β-dual polymorphic selectivity (denoted as dual-selective β-NA in this study)[58-61]; in the point view of geometric shape, DMDBS and DCNDCA are club-shaped, Pa-Ca is flaky staff, NAB83 is rod-like entities, and WBG-II is irregular block-like crystal. Meanwhile, the sizes of these NAs are also different from each other.

Table 1   Detailed information of the nucleating agents added in iPP

| Name	Trade name	Manufacturer	Chemical Composition	Polymorphic Selectivity
DMDBS	Millad 3988	Milliken Comp. USA.	Bis (3,4-dimethylobenzylideno) sorbitol.	α-single
Pa-Ca	-	Synthesized by neutralization of pimelic acid and calcium hydroxide in laboratory	Calcium pimelate [$C_7H_{10}O_4Ca$, pass through 200 mesh sieve (particle size $\leq$ 75 μm)]	β-single
NAB83	NAB83	Guangzhou Chenghe (GCH) Technology Comp., China	Metal carboxylate of tetrahydrophthalic anhydride. The substituent groups of R_{1-8} are independently selected from: hydrogen, C1-C9 alkyl group, hydroxyl, phenyl group and halogen, while M is metal cation selected from barium, calcium, magnesium, strontium and zinc.	β-single
DCNDCA	TMB-5	Shanxi Chemical Academe, China	N, N'-dicyclohexyl-2,6-naphthalenedicarboxamide.	α-/β-dual
WBG-II	WBG-II	Guangdong Winner Functional Materials Corp., China	A general formula of $Ca_xLa_{1-x}(LIG1)_m(LIG2)_n$, where x and $1 - x$ is the proportion of Ca^{2+} and La^{3+} ion in the complex, while LIG1 and LIG2 are respectively a dicarboxylic acid and amide-type ligand with coordination numbers of m and n.	α-/β-dual
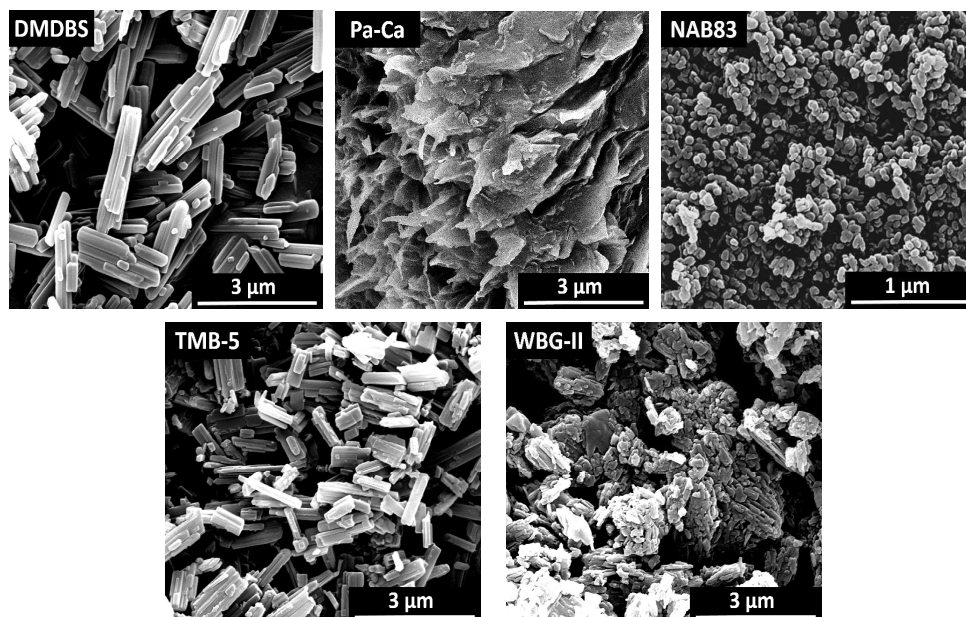
Figure 1   SEM images of the used nucleating agents.

2.2 Sample preparation

The iPP pellets and NA were mixed in the weight ratio of 100:1 and then extruded by a twin-screw extruder (SHJ-20, Nanjing Giant Machinery Co., Ltd, China) and pelletized to obtain master batch. The master batch and iPP were mixed and extruded by twin-screw again to obtain β-iPP. The concentration of each NA was 0.03 wt%.

2.3 Differential scanning calorimetry (DSC)

All the calorimetric experiments were performed with Mettler Toledo DSC1 (Mettler Corp., Swiss) differential scanning calorimeter (DSC) under nitrogen atmosphere (50 mL/min). The temperature scale calibration was performed using indium as a standard to ensure reliability of the data obtained. 5 mg round samples were used. All the thermograms were fitted using Peakfit 4.12 software according to literatures[62, 63]. In this way, the single melting curve of the β-iPP was separated into individual peaks and therefore the relative percentage of β-phase was calculated. The relative percentage crystallinities of α-crystal (α_c) and β-crystal (β_c) were estimated by the following expressions:

$$\alpha_c = X_\alpha / \left(X_\beta + X_\alpha \right) \tag{1}$$

$$\beta_c = X_\beta / \left(X_\beta + X_\alpha \right) \tag{2}$$

where the degree of crystallinities X_α and X_β associated with α-phase and β-phase, respectively.
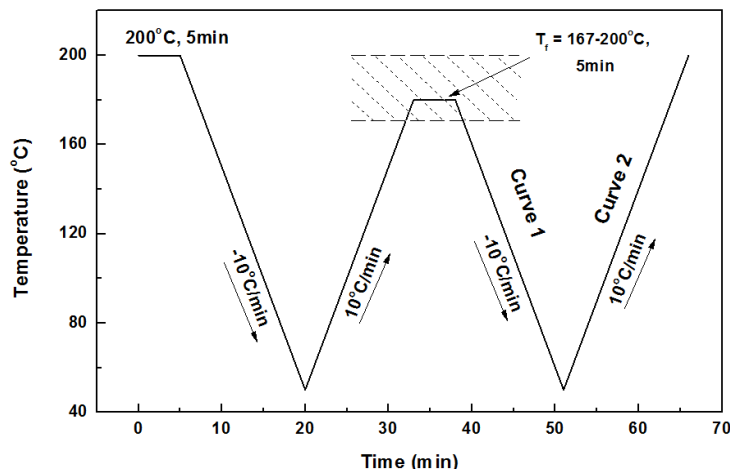
Scheme 1 Schematic illustration of the thermal protocol applied on the iPP samples

In DSC measurement, the thermal treatment described in Scheme 1 is applied to create iPP with different melt structures (namely, to tune the presence and amount of ordered structures in iPP melt). The sample is firstly heated to 200°C and held for 5min to erase any previous thermal history. Then it is cooled to 50°C at 10°C/min to create "standard" thermal history. After that, it is heated to different fusion temperatures (T_f, ranging from 167-200°C) at 10°C/min and held for 5min to create different melt structures, namely, to control the presence and content of the ordered structures in the melt. Then, it is cooled down to 50°C at 10°C/min. Finally, it is heated to 200°C at 10°C/min.

2.4 Wide-angle X-ray diffraction (WAXD)

WAXD patterns were recorded with a DX-1000 diffractometer. The wavelength of CuKα was λ=0.154 nm and the spectra were recorded in the 2θ range of 5–35°, a scanning rate of 2°/min, and a scanning step of 0.02°.

The content of the β-crystal was determined according to standard procedures described in the literatures[40, 64, 65], employing the following equation[36]:

$$k_\beta = \frac{H_\beta(110)}{H_\beta(110) + H_\alpha(110) + H_\alpha(040) + H_\alpha(130)} \tag{3}$$

7

k_β denotes the relative content of β-crystal form (WAXD), $H_\alpha(110)$, $H_\alpha(040)$ and $H_\alpha(130)$ are the intensities of the strongest peaks of α-form attributed to the (110), (040) and (130) planes of monoclinic cell, respectively. $H_\beta(110)$ is the intensity of the strongest (110) diffraction peak of the trigonal β-form[31, 33].

2.5 Polarized optical microscopy (PLOM)

The morphology evolution during crystallization was studied with a ZEISS MC-80 polarized light microscope equipped with a LINKAMTP-91 hot-stage and a camera system (ZEISS Co. Ltd., Germany). To enhance contrast, a λ wave plate was inserted between the polarizers.

2.6 Scanning electron microscopy (SEM)

The morphology observation (Scanning Electronic Microscopy, SEM) was performed on a JSM-5900 LV environmental scanning electron microscope at an accelerating voltage of 20 kV. Before SEM characterizations, the surfaces of all the samples were coated with a thin layer of gold by ion sputtering. All the samples were etched for 2h in a solution containing 1.3 wt% potassium permanganate (KM_nO_4), 32.9 wt% concentrated sulfuric acid (H_2SO_4) and 65.8 wt% concentrated phosphoric acid (H_3PO_4), according to the procedure proposed by Olley and Bassett[66].

2.7 Rheological measurement

The rheological measurements were performed with a stress-controlled Gemini 200 rheometer (Malvern Instruments Ltd, UK) in the linear viscoelastic regime under a nitrogen atmosphere, and the selected stress was 10 Pa. Testing sample disks with a diameter of 25 mm and a thickness of 1.5 mm were prepared by compression molding of the PP pellets at 190°C for 5 min. Each specimen was initially heated to 220°C and held for 5 min. A dynamic temperature sweep mode was applied at an oscillation frequency of 0.1 rad/sec, and the temperature was subsequently decreased at a rate of 3°C/min until the solidification of iPP occurred.

3. Results and Discussion

### 3.1 Preliminary analysis of the crystallization behavior

The influence of the nucleating agents (NAs) on the crystallization and melting behavior of iPP is studied by means of DSC and WAXD. Figure 2 shows the DSC

cooling curves and subsequent heating curves, and the WAXD profiles of the samples with the same thermal history. The crystallization temperature (T_c) on DSC cooling curves, the relative percentage of β-phase calculated from DSC heating curves ($β_c$) and WAXD profiles are shown in Figure 3a-c, respectively. Note that multiple peaks emerge on the DSC heating profiles of some samples. According to the literatures[36, 67] and the WAXD results in Figure 2c, the melting peaks in the temperature range lower than 155°C are classified as β-phase melting peaks, while the melting peaks emerge above 155°C are the α-phase melting peaks.

On the cooling curves, the T_c increases after the addition of each NA due to the nucleating effects. Meanwhile, on the DSC heating curves and WAXD profiles (Figure 2b and 2c), the polymorphic behavior of the nucleated iPP is greatly dependent on the characteristic of the NAs: β-crystallization cannot take place in DMDBS-nucleated iPP due to its α-single polymorphic selectivity; iPP nucleated with Pa-Ca and NAB83 show high β-phase proportion ($β_c$ from DSC and $K_β$ from WAXD), reflecting the high β-nucleation efficiency of the NAs; iPP nucleated with DCNDCA and WBG-II only form relative low proportion of β-phase since DCNDCA and WBG-II are dual-selective β-NAs having lower β-nucleation efficiency compared with NAB83 and Pa-Ca.
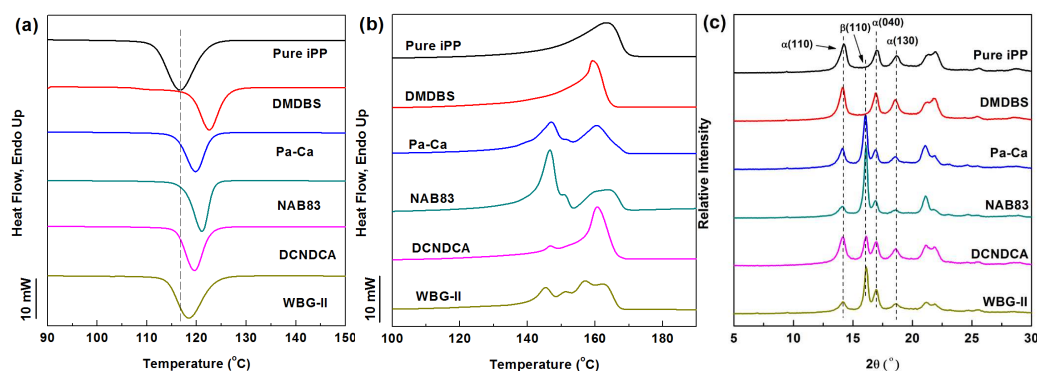
Figure 2 (a) cooling curves, (b) subsequent heating curves of the pure iPP and the nucleated iPP

samples and (c) the WAXD profiles of the samples with the sample thermal history.
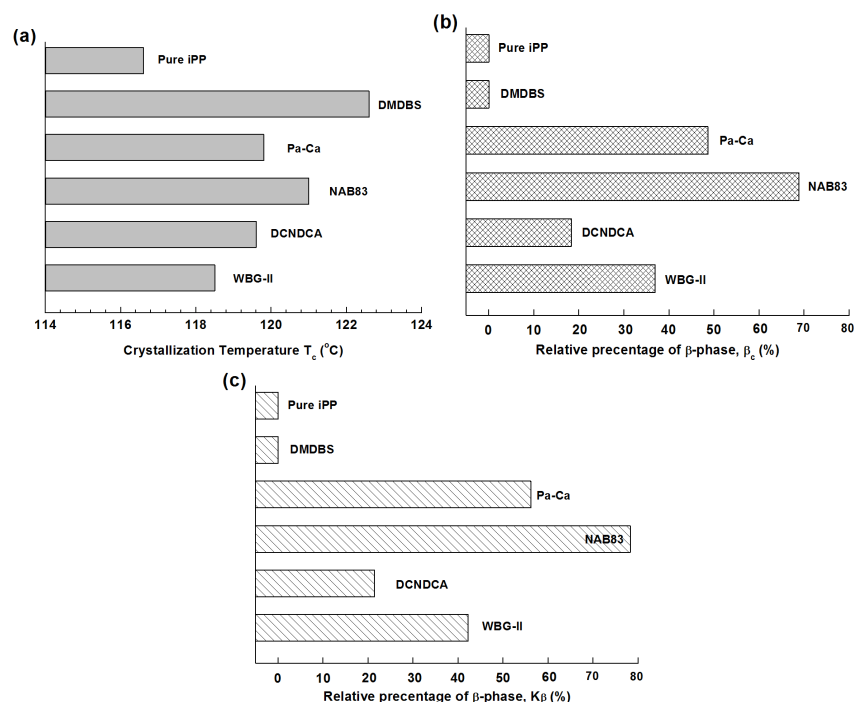
Figure 3 (a) the crystallization peak temperature, (b) relative percentage of β-phase (β$_c$)

calculated from DSC heating curves and (c) the β-phase proportion (K$_β$) calculated from the

WAXD profiles.

3.2 Crystallization behavior of nucleated iPP with different melt structures

By tuning the fusion temperature (T$_f$) using the thermal treatment protocol described in Scheme 1, the content of ordered structures in iPP melt is efficiently controlled. In this section, the crystallization behaviors of iPP samples with different contents of ordered structures are studied.

3.2.1 Crystallization behavior

Figure 4 shows the cooling curves (Curve 1 in Scheme 1) of the samples after held at different T$_f$. The variations of crystallization temperature T$_c$ as a function of T$_f$ is shown in Figure 5.
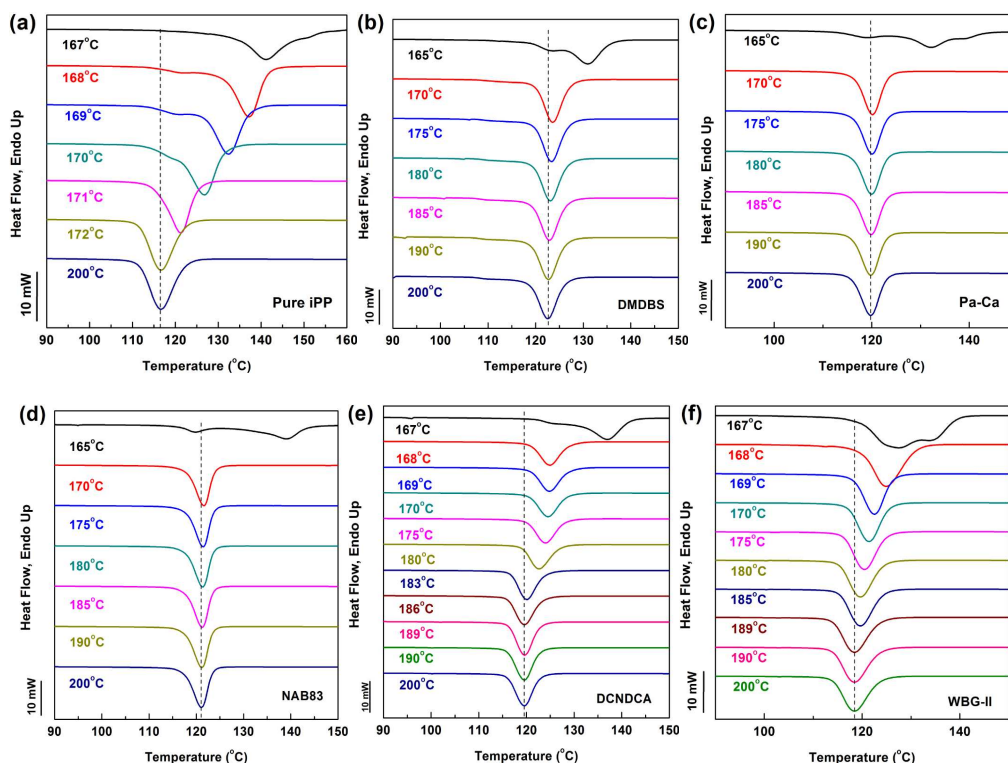
Figure 4   Cooling curves of the samples after held at different fusion temperatures T_f for 5 min.

The concentrations of the NAs are 0.03wt%, and the cooling rate is $10^oC/min$.
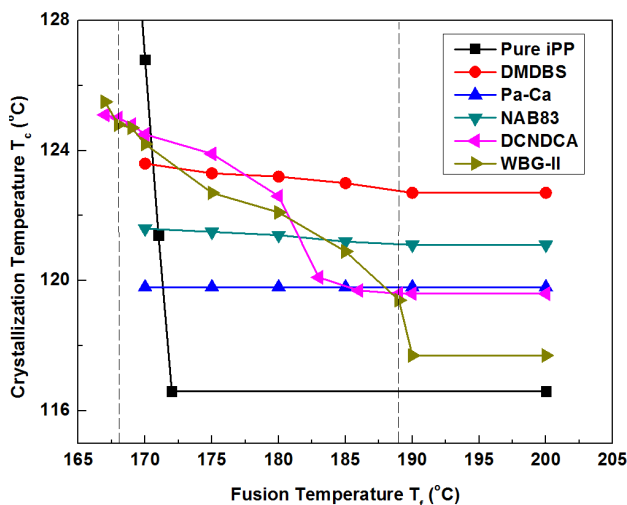
Figure 5   Variation of the crystallization temperature T_c as a function of fusion temperature T_f.

As can be seen from Figures 4 and 5, for Pure PP, when the T_f is higher than 171^oC, the crystallization temperature T_c stays almost constant, reflecting constant nucleation density of the melt, namely, iPP is fully molten; In the T_f range of 171-168^oC, T_c increases gradually with the decrease of T_f, indicating the presence of

11

the ordered structures in the melt and the occurrence of self-nucleation; as T_f decreases to lower than 168°C, the crystallization immediately happens during the subsequent cooling due to the presence of large ordered entities that can anneal or recrystallization during the cooling.

When the NA is added, for DMDBS, NAB83 and Pa-Ca, the crystallization peak temperature T_c stays almost unchanged with the decrease of T_f, indicating that for iPP nucleated with these NAs, the T_c is independent on T_f; however, for DCNDCA and WBG-II, an evident dependence of T_c on T_f is observed: when T_f is higher than 189 °C, T_c remains unchanged due to the constant nucleation density in the melt; when T_f is in the temperature range of 168-189 °C, the T_c increases gradually with the decrease of T_f due to the increase of the amount of ordered structures within the melt[18, 20, 21]; when T_f decreases to lower than 168°C, the crystallization peak significantly widens and two peaks can be observed, indicating that T_f is so low that the large ordered entities can survive in the melt[20], which are large enough to induce annealing or recrystallization in the course of subsequent cooling and therefore induce in a second crystallization peak in the high temperature range.

3.2.2 Melting behaviors

The heating curves of the samples are plotted in Figure 6. Figure 7 shows the relative percentages of the β-phase ($β_c$) of iPP nucleated with DCNDCA / WBG-II as a function of T_f. Meanwhile, Figure 8 is the WAXD profiles of iPP nucleated with DCNDCA / WBG-II after crystalized at the indicated T_f.
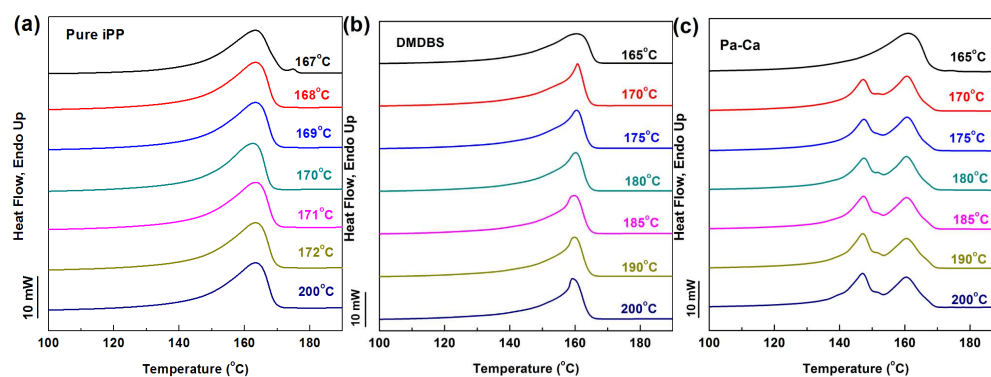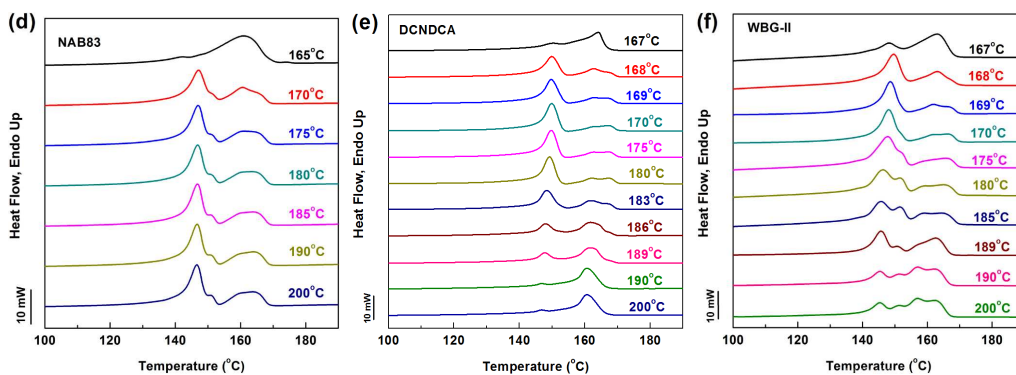
Figure 6   Heating curves (Curve 2 in Scheme 1) of (a) the Pure iPP and iPP nucleated with (b) DMDBS, (c) Pa-Ca, (d) NAB83, (e) DCNDCA and (f) WBG-II after held at the indicated T_f and then cooled to 50°C. The cooling and heating rates are 10°C/min.
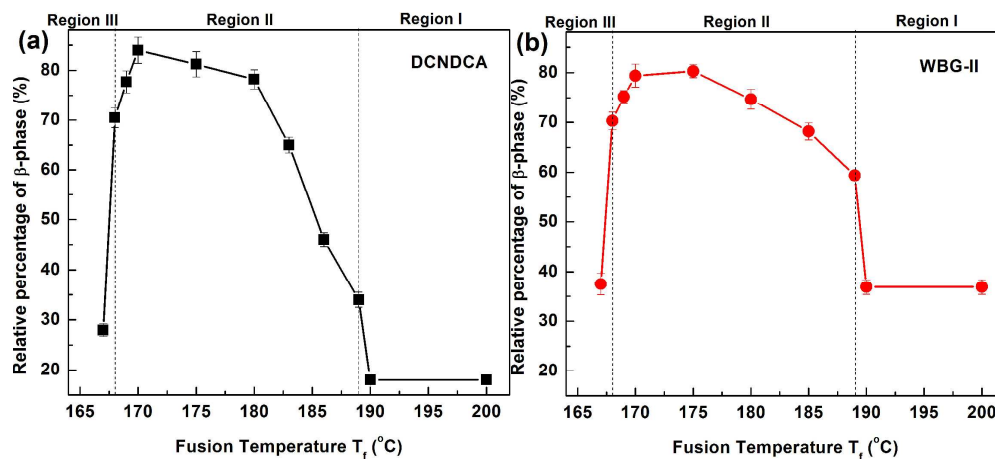
Figure 7   Plots of the relative contents of β-phase $β_c$ of iPP nucleated with (a) DCNDCA and (b) WBG-II as a function of the fusion temperature T_f. The error bars and statistics are also provided.
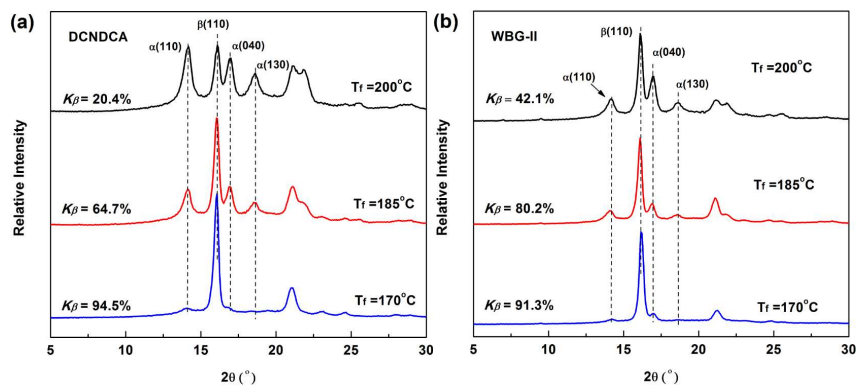
Figure 8   WAXD profiles of iPP nucleated with 0.03wt% (a) DCNDCA and (b) WBG-II

Figure 6a shows that for pure iPP, the melting profile stays constant when the T_f is higher than 167°C. When the T_f decreases to 167°C and lower, a small melting peak is observed at high melting temperature range, corresponding to the melting of the thick lamellaes due to the annealing and recrystallization of the survived large ordered entities at high temperature[20, 21]. The crystallization and melting behavior of pure iPP is well agreed with the conventional self-nucleation behavior of iPP in previous studies.

On the other hand, the melting profiles of iPP nucleated with DMDBS, Pa-Ca and NAB83 (Figure 6 b-d) stay almost unchanged when T_f varies in the temperature range of 170-200°C. As the T_f decreases to 165 °C, the β-melting peak located at 140-155°C disappears attributed to the depression effect of the survived large ordered entities on β-crystallization. The β-crystallization behaviors of iPP nucleated with DMDBS, Pa-Ca and NAB83 are in accord with the previous studies, showing that in these cases the used NAs cannot trigger any β-nucleation efficiency of the ordered structure.

For iPP nucleated with DCNDCA / WBG-II (Figure 6 e, f), when T_f is higher than 189°C, the sample is fully melting, the relative percentages of β-phase ($β_c$) on the heating curve is relatively low; surprisingly, when T_f is in the temperature range of 168-189°C, the β-melting peak becomes evidently shaper; meanwhile the $β_c$ increases significantly for iPP nucleated with DCNDCA and WBG-II, from 18.2% and 36.6% (when T_f is higher than 189°C) to 84.1% and 80.3% at maximum, respectively; When T_f is not higher than 167°C, $β_c$ decreases sharply due to the α-nucleation effect from the survived large ordered entities as mentioned above. The surprising results above indicate that the polymorphic behavior of iPP nucleated with DCNDCA/WBG-II is greatly dependent on the fusion temperature T_f, in another word, the presence of ordered structures in the melt. There exists a synergetic effect between the specific β-NA of DCNDCA/WBG-II and the ordered structures of iPP, which can evidently increase the β-nucleation efficiency of the sample.

According to the variation of crystallization peak temperature T_c on the cooling curves and the relative percentage of β-phase ($β_c$) on the DSC heating curves with the

change of fusion temperature (T_f), the whole T_f temperature range can be divided in to three regions as indicated by the dotted lines in Figure 7:

(i) Region I ($T_f > 189^oC$ in this study), where iPP is fully molten, the nucleation density in the melt is constant, T_c and β_c are constant;

(ii) Region II ($168^oC \leq T_f \leq 189^oC$), where the iPP is partially melting and an amount of ordered structures survive in the melt. Under the synergetic effect between the specific β-NA and the ordered structures of iPP, the β-nucleation efficiency of the sample is evidently elevated, resulting in the increase of T_c and β_c;

(iii) Region III ($T_f < 168^oC$)，where the large ordered entities that can induce annealing or recrystallization during the subsequent cooling can survive in the melt, resulting in emergence of second crystallization peak and the sharp decrease of β_c.

To benefit discussion, the synergetic effect between the specific β-NA and the ordered structures of iPP when the T_f is in Region II is named as the Ordered Structure Effect (OSE).

3.3 Effect of the supercooled treatment and holding time at fusion temperature

In order to obtain more understanding in the OSE, iPP nucleated with 0.03wt% WBG-II is selected as a representative sample, and two comparative studies are performed according to the thermal treatment protocols shown in Figure 9 (a) and (b). In Thermal Treatment 2 (Figure 9(a)), the sample is firstly heated to 200^oC and held for 5min to erase any previous history, then it is cooled to the indicated temperature (ranging from $168\text{-}200^oC$) and held for 5 min there, in order to create the iPP melt with different supercooled degree. Then it is cooled to 50^oC and subsequently heated to 200^oC. All the cooling and heating rates are $10^oC/min$. The obtained results (Figure 9(c)-(d)) show that the cooling and heating curves of the sample are not influenced by the supercooled degree, and are similar with those under the thermal treatment of direct cooling from 200^oC. Namely, without the presence of ordered structures in the melt, the sample nucleated with WBG-II cannot exhibit extra β-phase selectivity when the supercooled degree varies. The evident increase of the β-phase proportion in Figures 6-8 is attributed to the synergetic effect between the ordered structures of iPP

and the specific β-NA of DCNDCA and WBG-II.
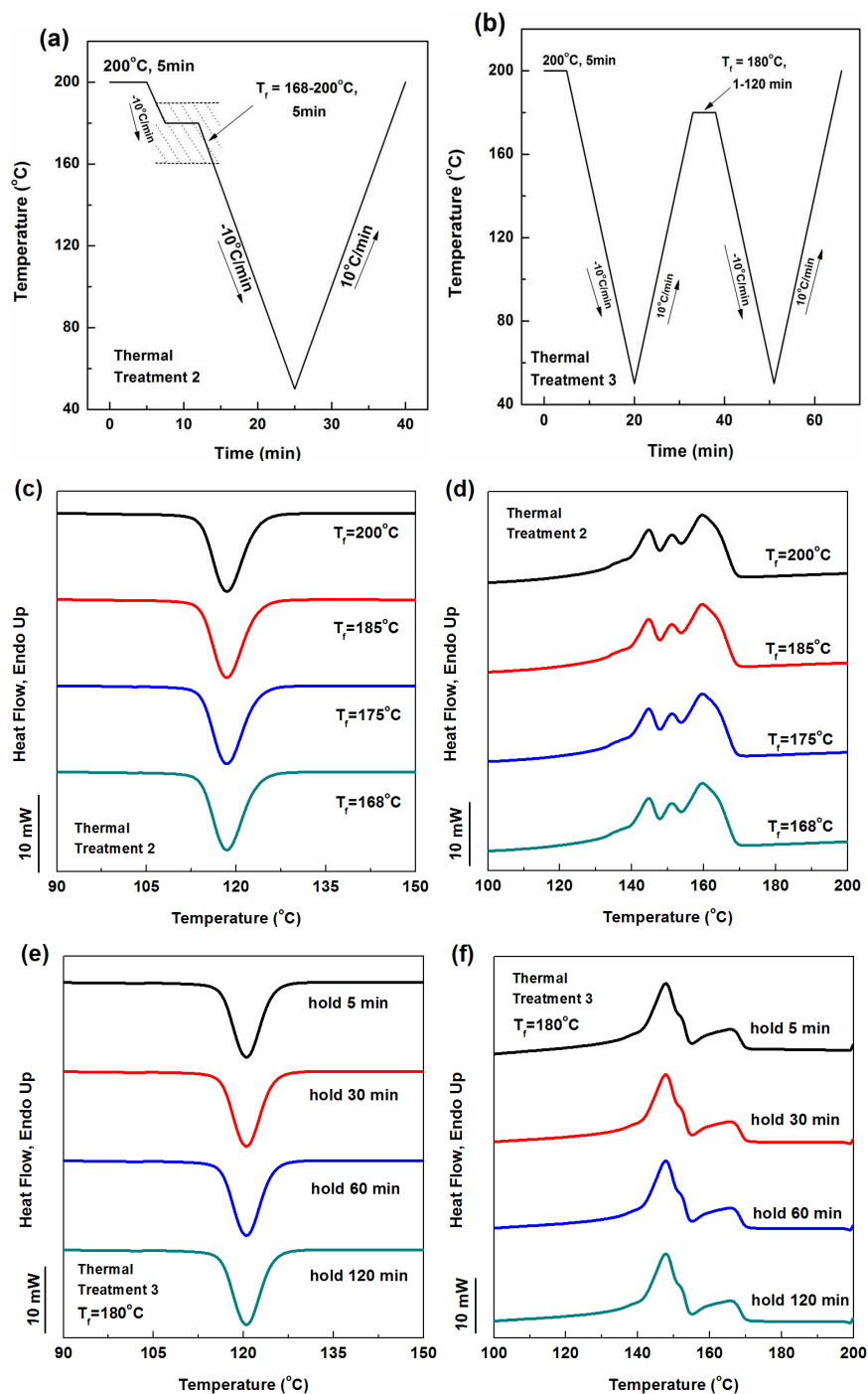
Figure 9   Comparative thermal treatment studies on the β-nucleated iPP samples with 0.03wt% WBG-II. (a) Thermal Treatment 2 without creation of the ordered structures within partial melt, (b) Thermal Treatment 3, holding at T_f =180°C for 1-120min. (c)-(d) the obtained cooling curves and subsequent heating curves of Thermal Treatment 2, (e)-(f) the obtained cooling and subsequent heating curves of Thermal Treatment 3.

Previous studies have reported that the ordered structures survived in the melt are unstable, which will gradually disappear when the holding time at the fusion temperature is long enough[22]. In order to study the thermal stability of the ordered structure under the influence of the specific β-NAs, the Thermal Treatment 3 described in Figure 9(b) has been applied. As the fusion temperature T_f ranges from 168-186°C (in Figure 9(b), T_f is 180°C as a representative), the results (Figure 9e, f) elucidate that even holding at T_f in Region II for 120 min, the obtained cooling and heating curves remain almost unchanged, indicating that under the influence of the specific β-NAs, the ordered structures have high thermal stability and can survive in the melt for long time, which is quite different from ordered structure in pure iPP melt reported previously[21, 22] due to the presence of the specific β-NA (0.03wt% WBG-II).

3.4 Morphology and structure evolution during crystallization

3.4.1 Rheological measurement

Since the viscoelastic properties are highly sensitive to microstructural changes of semicrystalline polymers even at very low crystallinity, the rheological approaches have been proved to be effective methods for the investigation of polymer crystallization[59, 68]. From a viewpoint of rheology, polymer crystallization is simplified as liquid-to-solid transition or biphasic system, where the rigid crystals suspend in amorphous melt. The dynamic storage modulus and viscosity will proportionally increase with elevated solid-like degree (crystallinity). Therefore, the evolving spectrum of elastic modulus G' upon cooling can be used to describe the early stage of crystallization. The elastic modulus G' as a function of temperature for each sample is recorded during the cooling process as shown in Figure 10.

As the fusion temperature T_f varies from 200°C to 185 and 170°C, it can be seen that the inflection point of the curve gradually shift towards higher temperature, suggesting that the crystallization occurs at higher temperature due to the increase of the amount of ordered structures.
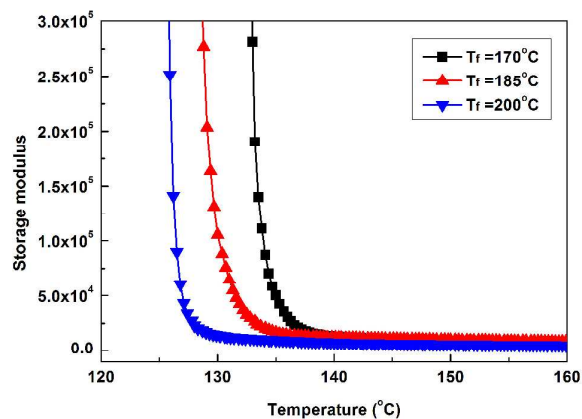
Figure 10   Storage modulus as a function of temperature of iPP nucleated with WBG-II cooled

from 200°C at the rate of 3°C/min.

3.4.2 PLOM observation

The online PLOM is performed to directly observe the morphology evolution of the sample. The obtained PLOM images of the sample during cooling process after held at different T_fs (170, 185, 200°C, respectively) are shown in Figure 11. Additional experimental results showed that the bright crystals are β-phase while the dark ones are α-crystals.

$T_f = 200^oC$

$T_f = 185^oC$
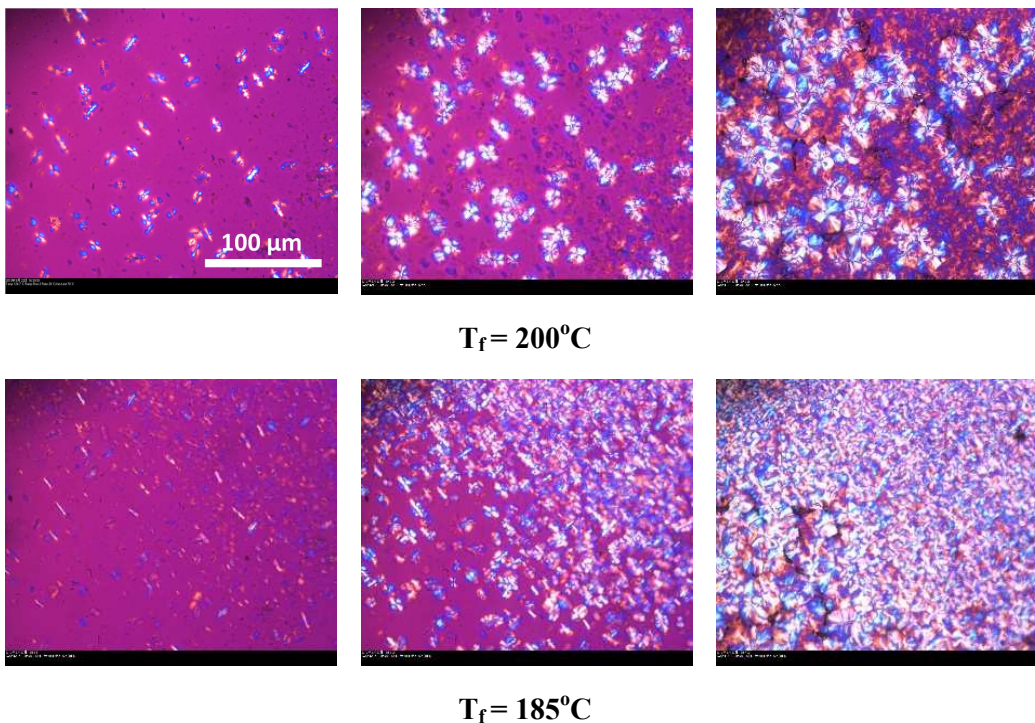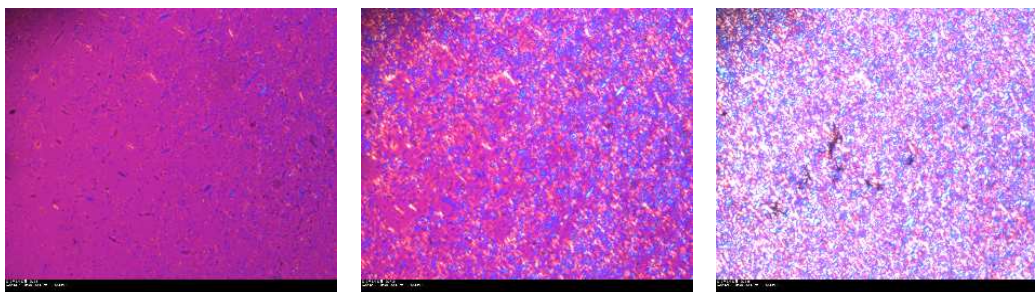
$$T_f = 170^oC$$

Figure 11   PLOM images of iPP/WBG-II cooled from after held at the indicated fusion temperature T_f (170, 185 and 200^oC, respectively). The cooling rate applied is 5^oC/min. The time interval between each set of data was 40 seconds.

Figure 11 reveals that when $T_f = 200^oC$, two kinds of crystal embryos can be observed at the early stage of the crystallization: one is the bright, large crystal nucleated by the β-NA, the other is the small, dark crystal derived mainly from density fluctuation[20, 22, 67]. As the crystallization proceeds, these two kinds of crystal embryos grow gradually and form large-sized β- and α-crystals, respectively. Finally, a mixture of α- and β-phase with low β-phase content is obtained; When T_f is 185^oC, the density and location of crystal embryos nucleated by WBG-II is quite similar with the case of $T_f = 200^oC$. Meanwhile, more small crystal embryos can be observed. Surprisingly, a large part of these small, dark crystal embryos exhibit β-nucleation efficiency, resulting in mass of β-crystals as the crystallization proceeds. Finally, more β-phase with smaller sizes is obtained; When T_f is 170^oC, mass of small, uniformly distributed crystal embryos can be observed at the beginning of the crystallization. After crystallization, large amount of small-sized bright β-crystals almost fill up the screen, indicating the formation of high proportion of β-phase. It should be noted that these small, dark crystal embryos seem to be uniformly distributed in the melt, which are not intensively concentrated around the bright, large crystal embryos induced by the WBG-II, reflecting the typical characteristic of self-nucleation.

On the other hand, the addition experimental results of PLOM observation of the crystallization procedure of pure iPP under the same thermal treatment showed only

the elevated crystallization temperature, the increase of α-nucleation sites and the decrease of α-crystallite sizes, which is in accord with the classical self-nucleation behavior reported in the literatures[18, 22].

The PLOM results above indicate that when T_f is in Region II (170, 185°C), the β-phase proportion is enhanced because the ordered structures survived in the partial melt have high β-nucleation efficiency. This is the first report of the presence of ordered structures with high β-selectivity in the quiescent iPP melt. Although the physical nature of this phenomenon still not clear enough, a basic principle of this phenomenon is evidently observed: in the absence of the specific β-NA, the ordered structures within the quiescent partial melt have no β-nucleation efficiency and cannot induce β-crystallization; with the help of the specific β-NA, the ordered structures turns to possess β-nucleation efficiency, i.e., the presence of specific β-NA plays a key role in this process. In general, a synergetic effect takes place between the specific β-NA and the ordered structures of iPP, resulting in the high β-nucleation efficiency of the ordered structures, and therefore significantly enhances the β-crystallization of the sample.

3.4.3 SEM

The SEM morphological result of the hot-molded samples after etching is shown in Figure 12.

$T_f = 200$ $^{\circ}$C

$$T_f = 185\ ^oC$$
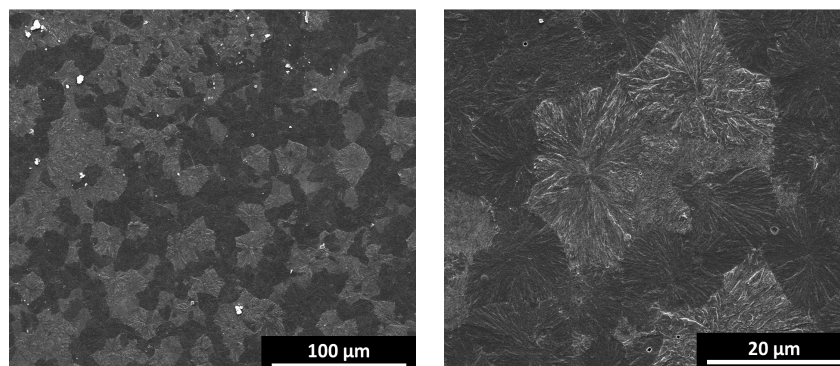
$$T_f = 170^oC$$
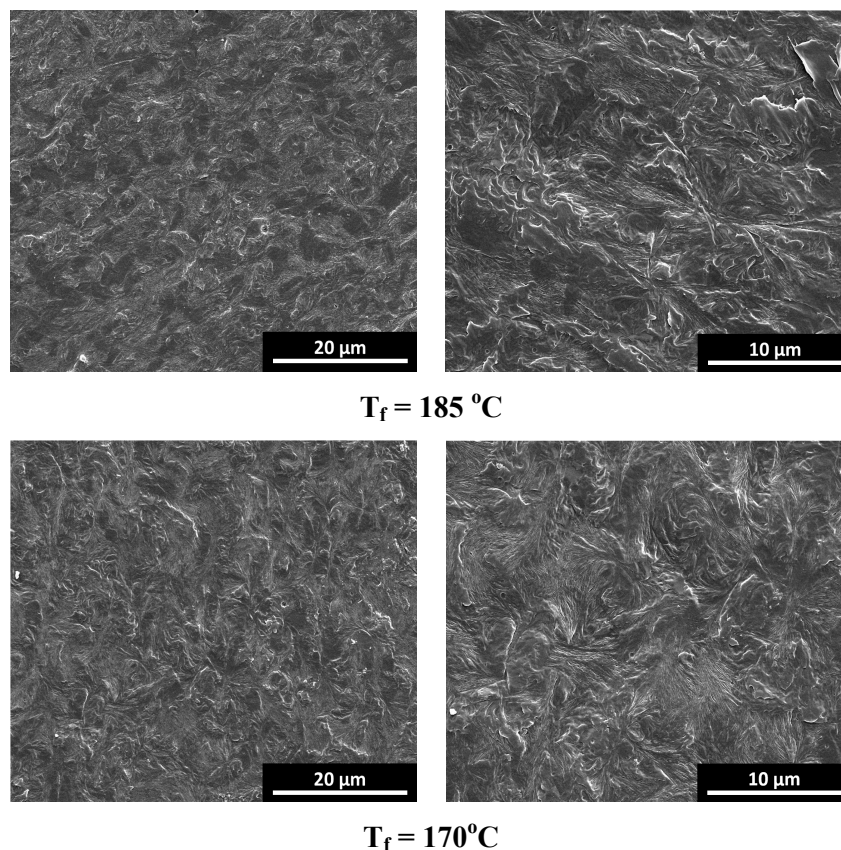
Figure 12   SEM images (after etching) of the iPP nucleated with 0.03wt% WBG-II after held at the indicated fusion temperature (T_f) for 5min and then cooling to room temperature.

When T_f =200°C, large spherulites with diameter about 20μm can be observed, meanwhile, the β-phase (bright spherulites in the SEM image)[69-71] content is relative low; As T_f comes to 185 and 170°C, the spherulite sizes decrease sharply and the β-phase content increase significantly. It should be noted that in all SEM images, only the β-spherulits can be observed.

3.6 Discussions

### 3.6.1 The key characteristic of β-NA in Ordered Structure Effect of iPP

The above results illustrated that only in the presence of DCNDCA/WBG-II can the synergetic effect between the β-NA and the ordered structures of iPP take places, resulting in the occurrence of the Ordered Structure Effect (OSE) as observed above. Considering the characteristics of the used five types of NAs such as the polymorphic

selectivity (Table 1), geometric shape (Figure 3) and β-nucleation efficiency (Figure 2), it can be preliminarily concluded that the general characteristic between DCNDCA and WBG-II is the α-/β-dual polymorphic selectivity (dual-selective β-NA), which might be the key characteristic of the β-NA for the occurrence of Ordered Structure Effect (OSE).

3.6.2 The role of ordered structure in early stage of β-crystallization

The experimental results also demonstrate that the ordered structures play an important role in the β-crystallization of iPP nucleated with dual-selective β-NA (β-NA with α-/β-dual polymorphic selectivity). A possible mechanism is proposed in Figure 13.
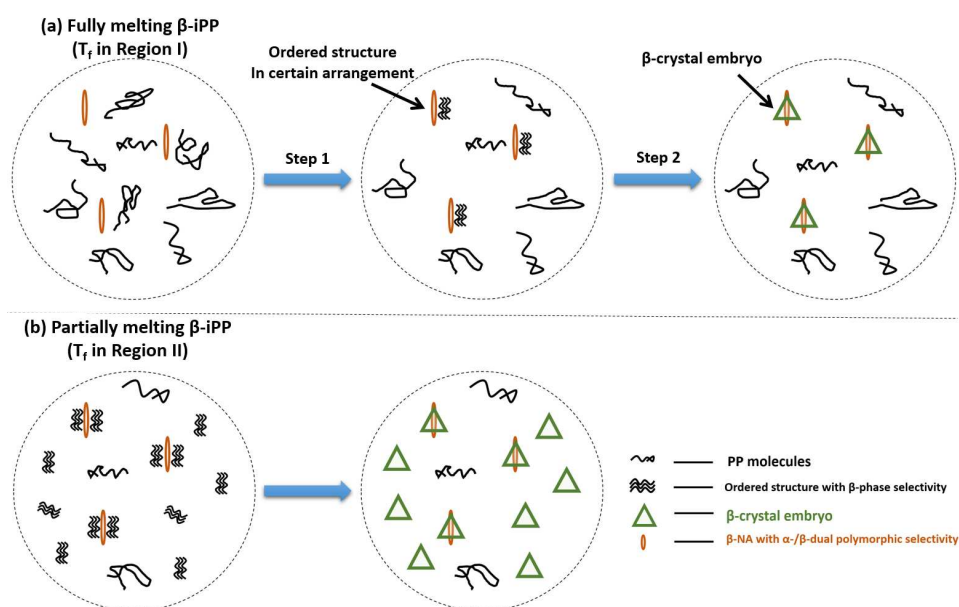
Figure 13   Schematic illustration of the two-stage β-nucleation mechanism of β-iPP nucleated with dual-selective β-nucleating agent.

Figure 13a shows for fully melting β-iPP (namely, the fusion temperature T_f is in Region I), the β-crystallization might take place in a two-step manner: in Step 1, under the influence of the dual-selective β-NA, the disordered iPP chains arrange into locally ordered structures, which have high β-nucleation efficiency; in Step 2, the

ordered structures having high β-nucleation efficiency encourage the occurrence of β-crystallization.

In Figure 13b, by tuning the T_f, the content of ordered structures in the iPP melt is intentionally controlled. In this way, the amount of ordered structures in iPP during the early stage of crystallization is significantly elevated. Under the influence of the dual-selective β-NA, the ordered structures may exhibit β-nucleation efficiency, therefore, the β-nucleation efficiency of the sample is significantly enhanced, resulting in the significant increase of β-phase proportion.

3.6.3 The interaction between ordered structure and dual-selective β-NA

It is reported that the ordered structures in certain orientation window can exhibit β-nucleation efficiency and therefore encourage the β-crystallization of iPP, showing a general characteristic of two-stage β-nucleation behavior: at the early stage of crystallization, the row nucleated α-lamellae firstly forms along the shear stress/fiber direction. Then, the β-nucleation takes place on the edge of the row nucleated α-lamellae and a competitive growth of both α- and β-crystal occurs.

Interestingly, Varga J[58], Yu J[61, 72], Qiang F et al.[59, 60] investigated the β-crystallization behavior of iPP nucleated with several types of dual-selective β-NAs, showing that these β-NAs have many similarities such as solubility in iPP matrix, self-assemble behavior; they can encourage both the α- and β-nucleation in similar manner. Moreover, Varga J[58] found that the lateral surface of DCNDCA leads a two-stage β-nucleation, which is surprisingly similar to that induced by the ordered structures in certain orientation window: at the early stage of crystallization, the row nucleated α-lamellae firstly forms along the side surface of the NA. After that, the β-nucleation takes place on the edge of the row nucleated α-lamellae and then a competitive growth of both α- and β-crystal occurs.

Based on the studies concerning the β-crystallization induced by orientated locally ordered structure and the dual-selective β-NAs, a possible explanation of the interaction between ordered structure and the dual-selective β-NAs is: the presence of dual-selective β-NAs might enable the ordered structures to possess certain

orientation status and therefore exhibit high β-nucleation efficiency. In another word, the β-nucleation of iPP in the cases such as crystallization under shear stress / oriented iPP homogeneous fiber and the addition of dual-selective β-NA may have the same nature; meanwhile, the ordered structure in certain orientation status is the crucial factor in all of these cases.

On the other hand, since the concentration of the dual-selective β-NA is directly related to the interaction between iPP chains and the β-NA, it might be a key factor in the occurrence of the Ordered Structure Effect (OSE), which can explain why previous studies with the addition of high β-NA concentration cannot induce the OSE observed in this study. The role of β-NA concentration in OSE of iPP should be further investigated.

4. Conclusions

In this study, we selected five types of representative nucleating agent (NA) and investigated their influence on the crystallization and polymorphic behavior of iPP with different melt structures (i.e., the amount of ordered structures), by means of DSC, WAXD, PLOM, SEM and rheological measurement. It was found that a synergetic effect between the ordered structures of iPP and the β-NA with α-/β-dual selectivity (dual-selective β-NA) takes place, resulting in an evident enhancement of the β-nucleation efficiency of the samples and great increase of the β-phase proportion, which is called the Ordered Structure Effect (OSE). The ordered structures in iPP melt play a determining role in the β-nucleation process of iPP nucleated with dual-selective β-NAs, meanwhile, the dual-selective β-NA provide the ordered structures certain influence, making them showing high β-nucleation efficiency. A possible mechanism was proposed.

References

1. G. Strobl, *Eur. Phys. J. E*, 2000, 3, 165-183.
2. J. J. I. Lauritzen and J. D. Hoffman, *Journal of Applied Physics*, 1973, 44, 4340-4352.
3. B. Lotz, *European Physical Journal E*, 2000, 3, 185-194.
4. M. Muthukumar, *European Physical Journal E*, 3, 199-202.
5. L. Li and W. de Jeu, in *Interphases and Mesophases in Polymer Crystallization II*, Springer Berlin Heidelberg, 2005, vol. 181, ch. 107175, pp. 75-120.
6. S. Z. D. Cheng, C. Y. Li and L. Zhu, *European Physical Journal E*, 2000, 3, 195-197.
7. G. Strobl, *Progress in Polymer Science*, 2006, 31, 398-442.
8. J. D. Hoffman and R. L. Miller, *Polymer*, 1997, 38, 3151-3212.
9. R. H. Gee, N. Lacevic and L. E. Fried, *Nature Materials*, 2006, 5, 39-43.
10. A. Sanz, A. Nogales, I. Puente-Orench, M. Jimenez-Ruiz and T. A. Ezquerra, *Physical Review Letters*, 2011, 107.
11. M. Soccio, A. Nogales, N. Lotti, A. Munari and T. Ezquerra, *Physical Review Letters*, 2007, 98.
12. T. K. G. Matsuba, M. Saito, K. Kaji, K. Nishida, *Physical Review E*, 2000, 62, 1-4.
13. C. L. Nitash P. Balsara, *Physical Review Letters*, 1996, 77, 3847-3850.
14. K. Kaji, K. Nishida, T. Kanaya, G. Matsuba, T. Konishi and M. Imai, 2005, 191, 187-240.
15. Y. Cong, Z. Hong, W. Zhou, W. Chen, F. Su, H. Li, X. Li, K. Yang, X. Yu, Z. Qi and L. Li, *Macromolecules*, 2012, 45, 8674-8680.
16. Y. Cong, Z. Hong, Z. Qi, W. Zhou, H. Li, H. Liu, W. Chen, X. Wang and L. Li, *Macromolecules*, 2010, 43, 9859-9864.
17. X. Li, F. Su, Y. Ji, N. Tian, J. Lu, Z. Wang, Z. Qi and L. Li, *Soft Matter*, 2013, 9, 8579-8588.
18. B. Fillon, J. Wittmann, B. Lotz and A. Thierry, *Journal of Polymer Science Part B: Polymer Physics*, 1993, 31, 1383-1393.
19. D. Cavallo, L. Gardella, G. Portale, A. J. Muller and G. C. Alfonso, *Polymer*, 2014, 55, 137-142.
20. A. J. Muller and M. L. Arnal, *Progress in Polymer Science*, 2005, 30, 559-603.
21. A. T. Lorenzo and A. J. Müller, *Journal of Polymer Science Part B: Polymer Physics*, 2008, 46, 1478-1487.
22. A. T. Lorenzo, M. L. Arnal, J. J. Sánchez and A. J. Muller, *Journal of Polymer Science Part B: Polymer Physics*, 2006, 44, 1738-1750.
23. B. Fillon, B. Lotz, A. Thierry and J. Wittmann, *Journal of Polymer Science Part B: Polymer Physics*, 1993, 31, 1395-1405.
24. J. Kang, B. Xiong, D. Liu, Y. Cao, J. Chen, F. Yang and M. Xiang, *Journal of Polymer Research*, 2014, 21, 1-10.
25. J. Kang, J. Li, S. Chen, S. Zhu, H. Li, Y. Cao, F. Yang and M. Xiang, *Journal of Applied Polymer Science*, 2013, 130, 25-38.
26. J. Kang, F. Yang, T. Wu, H. Li, D. Liu, Y. Cao and M. Xiang, *Journal of Applied Polymer Science*, 2012, 125, 3076-3083.
27. J. Kang, F. Yang, T. Wu, H. Li, Y. Cao and M. Xiang, *European Polymer Journal*, 2012, 48, 425-434.
28. J. Kang, Y. Cao, H. Li, J. Li, S. Chen, F. Yang and M. Xiang, *Journal of Polymer Research*, 2012, 19, 1-11.

29.   D. Liu, J. Kang, M. Xiang and Y. Cao, *Journal of Polymer Research*, 2013, 20.

30.   G. Natta and P. Corradini, *Nuovo Cim*, 1960, 15, 40-51.

31.   D. L. Dorset, M. P. McCourt, S. Kopp, M. Schumacher, T. Okihara and B. Lotz, *Polymer*, 1998, 39, 6331-6337.

32.   B. Fillon, A. Thierry, J. Wittmann and B. Lotz, *Journal of Polymer Science Part B: Polymer Physics*, 1993, 31, 1407-1424.

33.   D. R. Ferro, S. V. Meille and S. Bruckner, *Macromolecules*, 1998, 31, 6926-6934.

34.   S. Bruckner, P. J. Phillips, K. Mezghani and S. V. Meille, *Macromolecular Rapid Communications*, 1997, 18, 1-7.

35.   A. Nogales, B.S. Hsiao, R.H. Somani, S. Srinivas, A.H. Tsou, F.J. Balta-Calleja, T.A. Ezquerra, *Polymer*, 2001, 5247-5256.

36.   J. Varga, *Journal of Macromolecular Science, Part B*: *Polymer Physics*, 2002, 41, 1121-1171.

37.   S. G. Markus Blomenhofer, Doris Hanft, Hans-Werner Schmidt, Magnus Kristiansen, Paul Smith, Klaus Stoll, Dietmar Mader, and Kurt Hoffmann, *Macromolecules*, 2005, 38, 3688-3695.

38.   J. Kang, H. Peng, B. Wang, Z. Chen, J. Li, J. Chen, Y. Cao, H. Li, F. Yang and M. Xiang, *Journal of Applied Polymer Science*, 2014, 131, 40115.

39.   D. Libster, A. Aserin and N. Garti, *Polymers for Advanced Technologies*, 2007, 18, 685-695.

40.   H. Peng, B. Wang, J. Gai, J. Chen, F. Yang, Y. Cao, H. Li, J. Kang and M. Xiang, *Journal of Applied Polymer Science*, 2014, 131, 40027.

41.   J. Kang, B. Wang, H. Peng, J. Li, J. Chen, J. Gai, Y. Cao, H. Li, F. Yang and M. Xiang, *Polymers for Advanced Technologies*, 2014, 25, 97-107.

42.   J. Kang, Z. Chen, T. Zhou, F. Yang, J. Chen, Y. Cao and M. Xiang, *Journal of Polymer Research*, 2014, 21, 1-12.

43.   Z. Chen, B. Wang, J. Kang, H. Peng, J. Chen, F. Yang, Y. Cao, H. Li and M. Xiang, *Polymers for Advanced Technologies*, 2014, 25, 353-363.

44.   J. Kang, J. Gai, J. Li, S. Chen, H. Peng, B. Wang, Y. Cao, H. Li, J. Chen, F. Yang and M. Xiang, *Journal of Polymer Research*, 2013, 20, 1-11.

45.   A. Pawlak and E. Piorkowska, *Colloid and Polymer Science*, 2001, 279, 939-946.

46.   Q. Liu, X. Sun, H. Li and S. Yan, *Polymer*, 2013, 54, 4404-4421.

47.   H. Li and S. Yan, *Macromolecules*, 2011, 44, 417-428.

48.   H. Li, X. Sun, S. Yan and J. M. Schultz, *Macromolecules*, 2008, 41, 5062-5064.

49.   S. Cheng, W. Hu, Y. Ma and S. Yan, *Polymer*, 2007, 48, 4264-4270.

50.   H. Li, S. Jiang, J. Wang, D. Wang and S. Yan, *Macromolecules*, 2003, 36, 2802-2807.

51.   D. Cavallo, G. Portale, L. Balzano, F. Azzurri, W. Bras, G. W. Peters and G. C. Alfonso, *Macromolecules*, 2010, 43, 10208-10212.

52.   D. Cavallo, F. Azzurri, L. Balzano, S. r. S. Funari and G. C. Alfonso, *Macromolecules*, 2010, 43, 9394-9400.

53.   G. C. Alfonso. Fiorenza Azzurri, *Macromolecules*, 2005, 38, 1723-1728.

54.   B. Zhang, J. Chen, F. Ji, X. Zhang, G. Zheng and C. Shen, *Polymer*, 2012, 53, 1791-1800.

55.   B. Zhang, J. Chen, J. Cui, H. Zhang, F. Ji, G. Zheng, B. Heck, G. Reiter and C. Shen, *Macromolecules*, 2012, 45, 8933-8937.

56.   J. C. Wittmann and B. Lotz, *Progress in Polymer Science*, 1990, 15, 909-948.

57.   Z. Zhang, Y. Tao, Z. Yang and K. Mai, *European Polymer Journal*, 2008, 44, 1955-1961.

58.   J. Varga and A. Menyhard, *Macromolecules*, 2007, 40, 2422-2431.

59.   F. Luo, K. Wang, N. Ning, C. Geng, H. Deng, F. Chen, Q. Fu, Y. Qian and D. Zheng, *Polymers for Advanced Technologies*, 2011, 22, 2044-2054.

60.   F. Luo, C. Geng, K. Wang, H. Deng, F. Chen, Q. Fu and B. Na, *Macromolecules*, 2009, 42, 9325-9331.

61.   M. Dong, Z. Guo, Z. Su and J. Yu, *Journal of Applied Polymer Science*, 2011, 119, 1374-1382.

62.   Y. Yamamoto, Y. Inoue, T. Onai, C. Doshu, H. Takahashi and H. Uehara, *Macromolecules*, 2007, 40, 2745-2750.

63.   J. Kang, J. Chen, Y. Cao and H. Li, *Polymer*, 2010, 51, 249-256.

64.   A. Khare, A. Mitra and S. Radhakrishnan, *Journal of Materials Science*, 1996, 31, 5691-5695.

65.   J. Varga, *Journal of Materials Science*, 1992, 27, 2557-2579.

66.   R. H. Olley, D. C. Bassett and D. J. Blundell, *Polymer*, 1986, 27, 344-348.

67.   N. Pasquini and A. Addeo, *Polypropylene Handbook*, Hanser, 2005.

68.   K. Wang, C. Zhou, C. Tang, Q. Zhang, R. Du, Q. Fu and L. Li, *Polymer*, 2009, 50, 696-706.

69.   J. Scudla, M. Raab, K.-J. Eichhorn and A. Strachota, *Polymer*, 2003, 44, 4655-4664.

70.   J. Kotek, I. Kelnar, J. Baldrian and M. Raab, *European Polymer Journal*, 2004, 40, 679-684.

71.   W. L. C. J.X. Li, C.M. Chan, *Polymer*, 1999, 40, 2089-2102.

72.   M. Dong, Z. Guo, J. Yu and Z. Su, *Journal of Polymer Science Part B: Polymer Physics*, 2008, 46, 1725-1733.
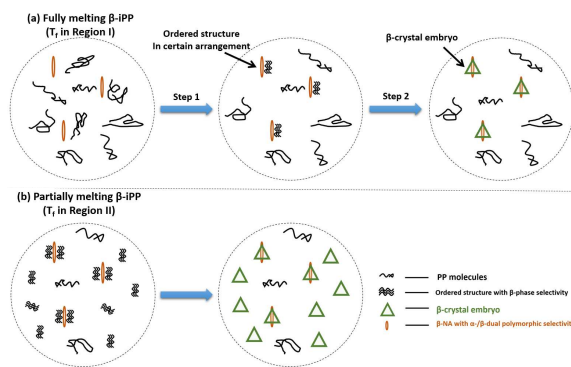
Schematic illustration of the two-stage β-nucleation mechanism of β-iPP nucleated with dual-selective β-nucleating agent and the role of ordered structures